

Initial State Quantum Fluctuations in the Little Bang

François Gelis¹ and Björn Schenke²

¹*Institut de physique théorique, CEA, CNRS, Université Paris-Saclay, F-91191 Gif-sur-Yvette, France*

²*Physics Department, Brookhaven National Laboratory, Upton, NY 11973, USA*

We review recent developments in the ab-initio theoretical description of the initial state in heavy-ion collisions. We emphasize the importance of fluctuations, both for the phenomenological description of experimental data from the Relativistic Heavy Ion Collider (RHIC) and the Large Hadron Collider (LHC), and the theoretical understanding of the non-equilibrium early time dynamics and thermalization of the medium.

Keywords: quantum chromo-dynamics, heavy ion collisions, quark-gluon plasma, hydrodynamics, thermalization

I. INTRODUCTION

Heavy Ion Collisions, devoted to probe the hot and dense phases of nuclear matter, may in principle be described by Quantum Chromodynamics (QCD) – the microscopic theory of quarks and gluons. However, due to the extremely complicated dynamics at play in the collisions, such an ab initio description appears hopeless. Instead, one resorts to various mesoscopic descriptions, that integrate out many of the microscopic details.

A crucial challenge in such a coarse graining procedure is to identify the relevant aspects of the underlying fundamental description that must be kept in order to correctly describe the system. In the underlying quantum field theory, renormalizability implies that quantum fluctuations are important down to spatial scales of the order of the typical inverse momentum, while smaller fluctuations are simply encapsulated in the scale dependence of a few parameters such as the coupling constant. But in the more macroscopic descriptions used in heavy ion collisions there is no such clear procedure.

The purpose of this review is to discuss the various sources of fluctuations, and their role in the observable outcome of the collisions.

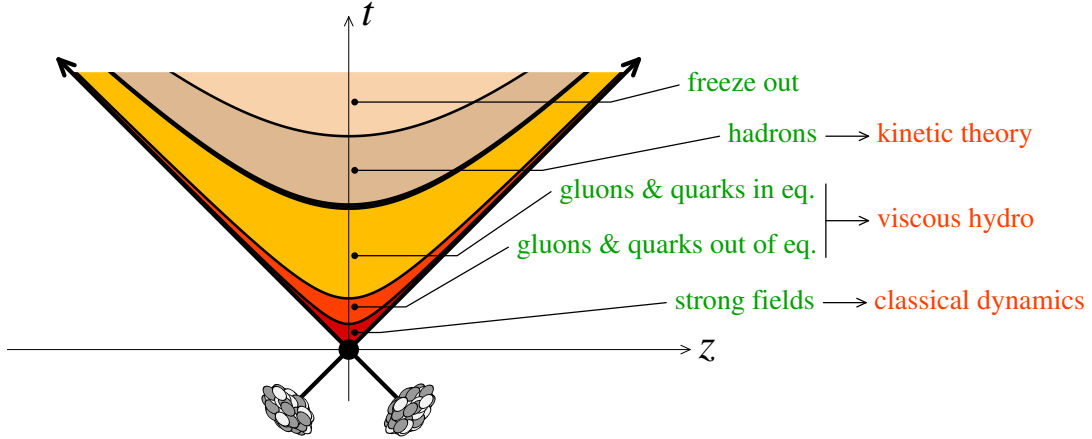


FIG. 1: Successive stages of a heavy ion collision.

A. Hydrodynamics in heavy ion collisions

Over many years, relativistic fluid dynamics has proven to be the most successful effective theory to describe the bulk dynamics of heavy ion collisions. Early on, ideal hydrodynamics was able to describe many qualitative features of the experimental data, including a large elliptic flow v_2 and mass splitting between the v_2 coefficients for different particle species. This gave the first indication that the matter created in heavy ion collisions at the Relativistic Heavy Ion Collider (RHIC) is close to a perfect fluid [1–3]. This was confirmed later at the Large Hadron Collider (LHC).

With the development of viscous relativistic hydrodynamic simulations and comparison to experimental data from heavy ion collisions [4] the value of the shear viscosity to entropy density ratio η/s could be determined to be close to the conjectured strong coupling limit of $\eta/s = 1/4\pi$ obtained from the AdS/CFT correspondence [5, 6]. Since then much progress has been made. In particular the inclusion of event-by-event fluctuations in the initial state of viscous hydrodynamics [7–9] has turned out to be of great importance. For recent reviews on the status of relativistic fluid dynamics for heavy ion collisions see [10–13].

B. Relevance of initial state fluctuations for data interpretation

The role of fluctuations in the transverse geometry of the collision system was realized when experimentally studying the elliptic flow in central Cu+Cu collisions at RHIC [14]. The large observed v_2 could only be explained when the shape of the overlap region was calculated relative to an axis determined by the fluctuating participants. This concept turned out to have far reaching consequences. In particular it allowed for the explanation of the structure of two particle correlations in their pseudo-rapidity η_p and azimuthal angular difference, namely the so called ridge. Its structure around $\Delta\phi = \pi$ in central collisions is due to the contribution of the odd harmonic v_3 , which in the absence of fluctuations would be zero [15–17].

The combined analysis of all v_n and their event-by-event distributions [18] has allowed to constrain the initial state and its fluctuations as well as the shear viscosity of the medium. The event-by-event distributions when scaled by the mean v_n are largely independent of the detailed transport parameters of the medium [19], which makes them ideal observables to constrain features of the initial state. In fact, currently there are only a few initial state models that describe all v_n distributions ($n = 2, 3, 4$) for all experimentally measured centralities. Most prominently, those are the IP-Glasma model [20–22], that we will discuss in more detail below, and the EKRT framework [23]. Both models include saturation effects and lead to similar energy deposition in the transverse plane. In [24] it was shown that the relevant feature to describe the experimental data is that the initial entropy density is proportional to the product of thickness functions.

In Section IID we will describe in more detail the relevance of the initial energy deposition and fluctuations for describing experimental data using the IP-Glasma model coupled to fluid dynamic calculations.

C. Fast thermalization: Is it necessary?

Hydrodynamics is an expansion around the energy momentum tensor of an ideal fluid¹ at rest. Since the baseline of this expansion is a fluid in local thermal equilibrium, it is often assumed that near-equilibrium is a prerequisite for hydrodynamics.

Data on flow observables indicate a very effective transfer from spatial anisotropy to momentum anisotropy. However, this transfer would be impaired by the strong dissipative effects that occur during the rearrangement of the internal degrees of freedom of an off-equilibrium system. Moreover, for a successful description of bulk observables in heavy ion collisions, the hydrodynamical evolution should start very shortly after the collision, at times $\tau \lesssim 1$ fm/c.

However, there is no direct evidence from data that the system is indeed close to equilibrium. Although the above argument suggests that a certain amount of pre-equilibration must have taken place before hydrodynamics becomes a valid description, there are examples (exactly solvable AdS/CFT models [32], or systems also studied in kinetic theory [33]) where the deviation of the energy-momentum tensor from its ideal form is of order one, and hydrodynamics nevertheless manages to track correctly the bulk evolution.

These examples suggest less stringent requirements: there should be a range of time where the pre-hydrodynamical description and hydrodynamics agree on the evolution of the stress tensor, even if it is still off-equilibrium. But even this weaker condition is hard to achieve in QCD. At leading order, QCD-based descriptions lead to an increasing bulk anisotropy, while it decreases in hydrodynamics. As we shall see later, higher order quantum fluctuations are essential in the isotropization of the stress tensor.

¹ In recent years, it has been proposed to expand around a fluid whose energy-momentum tensor is not isotropic [25–31].

II. INITIAL STATE IN 2 + 1 DIMENSIONAL CLASSICAL YANG-MILLS

A. QCD and Color Glass Condensate

Asymptotic freedom ensures that QCD perturbation theory can be used for processes involving a hard momentum scale. However, its applicability to the numerous softer particles is a priori questionable.

The gluon distribution in a hadron becomes large at small momentum fraction x and fixed transverse scale Q^{-1} . At fixed Q and decreasing x , gluons must eventually overlap in phase-space. When their occupation number is comparable to α_s^{-1} , gluon-gluon interactions become important. In particular, gluon recombinations tend to stabilize the occupation number, a phenomenon known as *gluon saturation*. New gluons can be produced only in the tail of the distribution, which is not yet saturated. Consequently, the typical gluon momentum increases with energy, leading to the saturation momentum $Q_s(x)$ depicted in Fig. 2. Moreover, thanks to asymptotic freedom, the corresponding value of the strong coupling constant decreases.

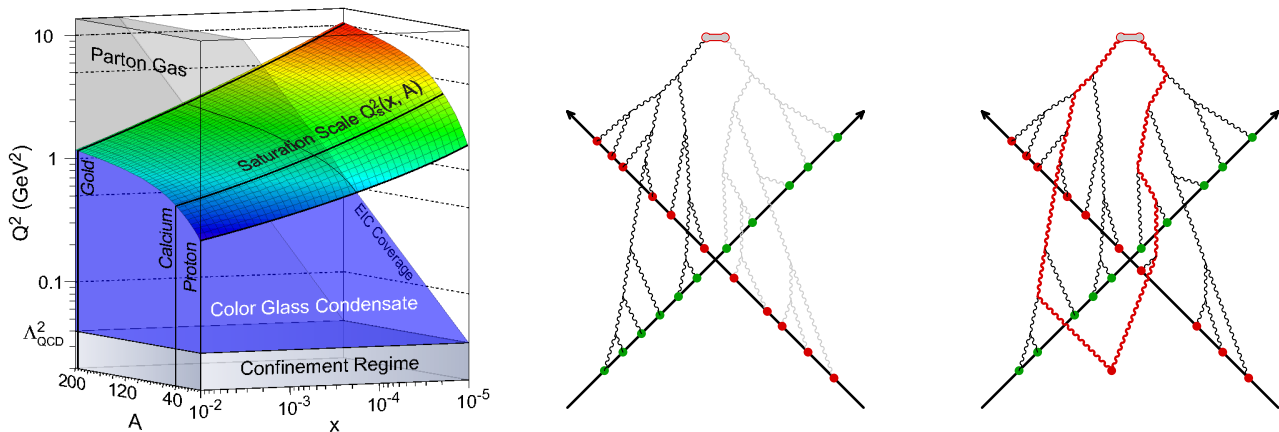


FIG. 2: Left: Saturation domain depending on x , Q and A . From [34]. Middle: Connected tree graphs that contribute to the single gluon spectrum at leading order (LO). The red and green dots denote the color sources of the two projectiles. Right: Same at NLO.

Gluons at the edge of saturation dominate scattering processes, allowing a weak coupling treatment for the calculation of the bulk of particle production. However, this system is non-perturbative, since a large occupation number of order α_s^{-1} compensates the smallness of the coupling. The *Color Glass Condensate* (CGC) is a QCD-based effective theory, designed to organize calculations in the saturation regime [35]. Its central idea is to use the large gluon occupation number in order to organize the expansion around classical solutions.

An observer in the center of momentum frame of a collision sees two streams of color charges flowing from opposite directions, that can be represented as two color currents J_1^μ and J_2^μ . At high energy, their dominant components are the $J^{\pm 2}$ ($J^{1,2}$ are inversely proportional to the collision energy, and thus neglected). Because of time dilation, the internal dynamics of the projectiles appears totally frozen to the observer, and therefore J_1^μ (resp. J_2^μ) is independent of x^+ (resp. x^-):

$$J_1^{\mu a}(x) = \delta^{\mu+} \rho_{1a}(x^-, \mathbf{x}_\perp) \quad , \quad J_2^{\mu a}(x) = \delta^{\mu-} \rho_{2a}(x^+, \mathbf{x}_\perp) \quad , \quad (1)$$

where the functions $\rho_{1,2}$ represent the density of color charges in the projectiles. These distributions reflect the configuration of the color charges just before the collision and are not known event-by-event, but one may develop a theory for its statistical distribution $W[\rho]$. The McLerran-Venugopalan [36, 37] model argues that in a nucleus with many colored constituents this distribution should be Gaussian. Moreover, thanks to confinement, this model neglects correlations between partons located at different transverse positions:

$$W[\rho] \equiv \exp \left\{ - \int d^2 \mathbf{x}_\perp \frac{\rho_a(x^-, \mathbf{x}_\perp) \rho_a(x^-, \mathbf{x}_\perp)}{2\mu^2(x^-, \mathbf{x}_\perp)} \right\} \quad , \quad (2)$$

² We use light-cone coordinates: $x^\pm \equiv (x^0 \pm x^3)/\sqrt{2}$.

where $\mu^2(x^-, \mathbf{x}_\perp)$ characterizes the local density of color charges.

Closer to the observer's rapidity, degrees of freedom should not be approximated by static sources, but treated as conventional quantum fields. Thus, the CGC is a Yang-Mills theory coupled to an external color current,

$$\mathcal{L}_{\text{CGC}} \equiv -\frac{1}{2} \text{tr} (F^{\mu\nu} F_{\mu\nu}) + J_\mu A^\mu . \quad (3)$$

The coupling $J_\mu A^\mu$ is eikonal because the two types of degrees of freedom have vastly different longitudinal momenta. In order to avoid contributions from loop corrections that are already included in the sources, CGC calculations beyond LO require the introduction of cutoffs (one for each projectile) in longitudinal momentum in order to properly separate sources from fields.

The order of magnitude of a connected graph \mathcal{G} is

$$\mathcal{O}(\mathcal{G}) = g^{-2} g^{n_E} g^{2n_L} (gJ)^{n_J} , \quad (4)$$

where n_E counts the external gluons, n_L the independent loops and n_J the sources $J_{1,2}^\mu$ in the graph. In the saturated regime, $gJ \sim g^0$, and the order of magnitude depends only on n_E and n_L . Infinitely many graphs, differing in the number of sources, contribute to a given order in α_s : despite a weak coupling, the CGC is non-perturbative.

Crucial simplifications occur for *inclusive observables*, obtained as an average over all final states. In particular, only connected graphs contribute to such observables. The simplest inclusive observable is the single gluon spectrum, obtained at leading order by summing all the tree graphs shown in Fig. 2. These tree graphs can be expressed in terms of a solution to the classical Yang-Mills equations,

$$[\mathcal{D}_\mu, \mathcal{F}^{\mu\nu}] = J_1^\nu + J_2^\nu , \quad \lim_{x^0 \rightarrow -\infty} \mathcal{A}^\mu(x) = 0 , \quad (5)$$

in the Fock-Schwinger gauge $x^+ A^- + x^- A^+ = 0$. Intuitively, the absence of constraints on the gauge field at $x^0 \rightarrow +\infty$ comes from the fact that one sums over all final states.

From this classical solution, the gluon spectrum at LO is given by

$$\left. \frac{dN_1}{dY d^2 \vec{p}_\perp} \right|_{\text{LO}} = \frac{1}{16\pi^3} \int_{x,y} e^{ip \cdot (x-y)} \square_x \square_y \sum_\lambda \epsilon_\lambda^\mu \epsilon_\lambda^\nu \mathcal{A}_\mu(x) \mathcal{A}_\nu(y) , \quad (6)$$

where \square_x is the D'Alembertian operator and the ϵ_λ^μ are polarization vectors. Likewise, the multi-gluon spectra read

$$\left. \frac{dN_n}{d^3 \mathbf{p}_1 \cdots d^3 \mathbf{p}_n} \right|_{\text{LO}} = \left. \frac{dN_1}{d^3 \mathbf{p}_1} \right|_{\text{LO}} \times \cdots \times \left. \frac{dN_1}{d^3 \mathbf{p}_n} \right|_{\text{LO}} . \quad (7)$$

Initial conditions for hydrodynamical models require the energy-momentum tensor, whose expression in terms of the classical chromo-electric and chromo-magnetic fields \mathbf{E}^i and \mathbf{B}^i read

$$T_{\text{LO}}^{00} = \frac{1}{2} [\mathbf{E}^2 + \mathbf{B}^2] \quad T_{\text{LO}}^{0i} = [\mathbf{E} \times \mathbf{B}]^i \quad (8)$$

$$T_{\text{LO}}^{ij} = \frac{\delta^{ij}}{2} [\mathbf{E}^2 + \mathbf{B}^2] - [\mathbf{E}^i \mathbf{E}^j + \mathbf{B}^i \mathbf{B}^j] . \quad (9)$$

B. Practical implementation

The non-linear Yang-Mills equations cannot be solved analytically in general. For numerical approaches, one should have in mind the following:

1. Since collisions at high energy are almost invariant under longitudinal boosts, it is natural to map the forward light-cone with proper-time ($\tau \equiv \sqrt{2x^+ x^-}$) and rapidity ($\eta \equiv \frac{1}{2} \log(x^+/x^-)$). The Yang-Mills equations do not depend on rapidity, and become 1+2 dimensional if their initial condition is itself independent of rapidity (which is the case in the CGC at LO).
2. The sources $\rho_{1,2}$ are singular on the light-cones $x^\pm = 0$, that divide space-time in four regions shown in Fig. 3 (left). The gauge potential \mathcal{A}^μ vanishes in region 0, and is known analytically in regions 1,2 [38]. In region 3, it is known analytically just above the light-cone, at $\tau = 0^+$ [39] :

$$\begin{aligned} A_0^i &= \alpha_1^i + \alpha_2^i \quad , \quad E_0^i = 0 \quad , \quad \alpha_n^i = \frac{i}{g} U_n^\dagger \partial^i U_n \quad (n = 1, 2) , \\ A_{0\eta} &= 0 \quad , \quad E_0^\eta = i \frac{g}{2} [\alpha_1^i, \alpha_2^i] , \end{aligned} \quad (10)$$

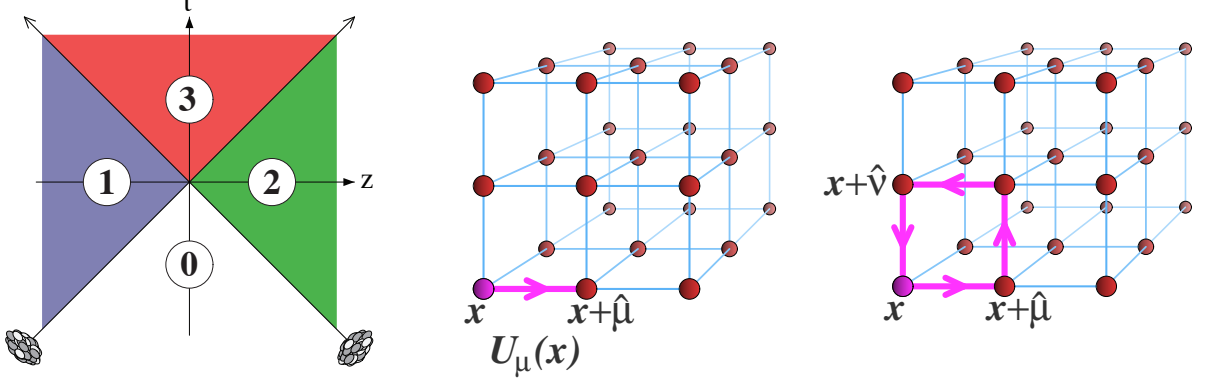


FIG. 3: Left: Space-time structure of the classical gauge field \mathcal{A}^μ . Middle and right: Link variable and plaquette on a 3-dimensional lattice.

where the Wilson line $U_1(\mathbf{x}_\perp)$ reads

$$V_1(\mathbf{x}_\perp) = \text{P} e^{ig \int dx^- \frac{1}{\nabla_\perp^2} \rho_1(x^-, \mathbf{x}_\perp)} \quad (11)$$

(and a similar expression for V_2 .)

Therefore, one needs to solve numerically 1+2-dim equations for $\tau > 0$ [40–49], with initial conditions (10) at $\tau = 0^+$. In practice, space is discretized on a lattice (see Fig. 3), while time remains a continuously varying variable. One uses Wilson’s formulation, where the gauge potentials A^μ are replaced by link variables (see Fig. 3), i.e. Wilson lines that span one elementary edge of the lattice

$$U_i(x) \equiv \text{P} \exp ig \int_x^{x+\hat{i}} ds A^i(s). \quad (12)$$

In contrast, the electrical fields E^i should be assigned to the nodes of the lattice, and the discretized Hamiltonian reads

$$\begin{aligned} \mathcal{H} = & \sum_{\vec{x}; i} \frac{E^i(\vec{x}) E^i(\vec{x})}{2} \\ & - \frac{6}{g^2} \sum_{\vec{x}; ij} 1 - \frac{1}{3} \text{Re} \text{Tr} \left(\underbrace{U_i(x) U_j(x + \hat{i}) U_i^\dagger(x + \hat{j}) U_j^\dagger(x)}_{\text{plaquette at the point } \vec{x} \text{ in the } ij \text{ plane}} \right). \end{aligned} \quad (13)$$

The corresponding Hamilton equations form a large but finite set of ordinary differential equations, that can be solved e.g. by the leapfrog algorithm.

Shortly after the collision (at $\tau \ll Q_s^{-1}$), the classical chromo-electric and chromo-magnetic fields are aligned with the collision axis [50]. The expectation value of transverse Wilson loops [51, 52],

$$W \equiv \left\langle \text{P} \exp ig \int_\gamma dx^i \mathcal{A}^i \right\rangle, \quad (14)$$

that measures the magnetic flux through the loop, provides information on the transverse correlation length of these fields. For large loops of area larger than Q_s^{-2} , W decreases approximately as $\exp(-\# \times \text{Area})$, indicating a decorrelation on transverse distances larger than Q_s^{-1} .

C. IP-Glasma framework

As discussed above, Yang-Mills equations for the boost invariant system have to be solved numerically, which has been done for homogeneous nuclei and $N_c = 2$ in [40] and for $N_c = 3$ in [43]. Finite size nuclei were studied in

[45, 48]. In particular, in [48] nucleons were sampled from a Woods-Saxon distribution and the color charge density of the nucleus was taken to be proportional to the sum of the thickness functions of all nucleons. Coulomb tails were avoided by implementing a color neutrality condition on length scales given by the inverse of Λ_{QCD} .

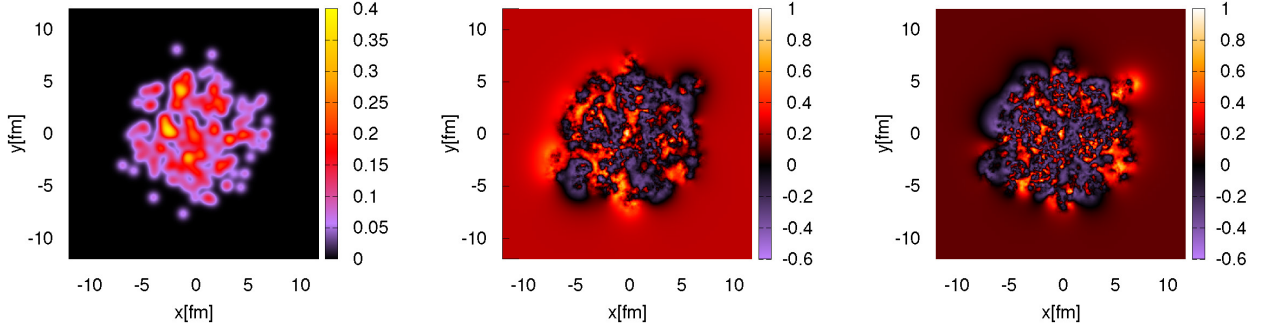


FIG. 4: Left: The incoming color charge density $g^2\mu^2$ for a gold nucleus at $\sqrt{s} = 200$ GeV. Middle: The correlator $(1/N_c)\text{Re}[\text{Tr}(V^\dagger(0,0)V(x,y))]$ showing the degree of correlations in the gluon fields for a gold ion at $\sqrt{s} = 200$ GeV at an x value that will contribute to gluon production at mid-rapidity. Right: Same as the middle figure but for $\sqrt{s} = 5$ TeV.

The IP-Glasma model [20, 21] is very similar to the framework introduced in [48]. The main differences are the use of the IP-Sat model [53, 54] to constrain the x and transverse position dependence of the color charge density using data from deeply inelastic scattering experiments, and the way one deals with the infrared tails. We now give a brief description of the various steps involved in computing the fluctuating initial state in the IP-Glasma model.

1. Nucleon positions \mathbf{x}_\perp^i ($i = 1 \dots A$) in the transverse plane of two nuclei are sampled from Woods-Saxon distributions with parameters adjusted to the nucleus of interest.
2. The sum of the Gaussian nucleon thickness functions T_p is computed. It enters the IP-Sat expression for the dipole cross section in deeply inelastic scattering [55]

$$\begin{aligned} \frac{1}{2} \frac{d\sigma_{\text{dip}}^A}{d^2\mathbf{x}_\perp}(\mathbf{r}_\perp, \mathbf{x}_\perp, x) &= \mathcal{N}_A(\mathbf{r}_\perp, \mathbf{x}_\perp, x) \\ &= \left[1 - e^{-\frac{\pi^2}{2N_c} \mathbf{r}_\perp^2 \alpha_s(Q^2) xg(x, Q^2) \sum_{i=1}^A T_p(\mathbf{x}_\perp - \mathbf{x}_\perp^i)} \right]. \end{aligned} \quad (15)$$

\mathcal{N}_A is the scattering amplitude of the nucleus, Q is the momentum scale related to the dipole size \mathbf{r}_\perp , $Q^2 = 4/\mathbf{r}_\perp^2 + Q_0^2$, with Q_0 fixed by the HERA inclusive data. In the first studies [20, 21], parameters were taken from the fit in Ref. [56], later [57] parameters from fits to high precision combined data from the H1 and ZEUS collaborations [58] were used. The gluon distribution $xg(x, Q^2)$ is parameterized at the initial scale Q_0^2 as $xg(x, Q_0^2) = A_g x^{-\lambda_g} (1-x)^{5.6}$ and then evolved up to the scale Q^2 using LO DGLAP-evolution. Like Q_0 , A_g and λ_g are constrained by the fit to HERA data.

3. Using the definition of the nuclear saturation scale Q_s as the inverse value of $r = \sqrt{\mathbf{r}_\perp^2}$ for which $\mathcal{N}_A = 1 - e^{-1/2}$, $Q_s(\mathbf{x}_\perp, x)$ is extracted. Using their proportionality, the color charge squared per unit area $g^2\mu^2(\mathbf{x}_\perp, x)$ is obtained from $Q_s(\mathbf{x}_\perp, x)$. The proportionality factor depends on the details of the calculation [59] and in the IP-Glasma calculations it is allowed to be varied in order to reproduce the overall normalization of produced particles [21]. A typical distribution of $g^2\mu^2(\mathbf{x}_\perp)$ is shown in Fig. 4 (left).
4. For a given x , which depends on the energy of the collision and the rapidity of interest, color charges $\rho^a(\mathbf{x}_\perp)$ are sampled from the distribution (2).
5. Assuming a finite width of the nucleus, the discretized version of the Wilson line (11) is given by [59]

$$V(\mathbf{x}_\perp) = \prod_{k=1}^{N_y} \exp\left(-ig \frac{\rho_k(\mathbf{x}_\perp)}{\nabla_\perp^2 + m^2}\right), \quad (16)$$

where $m \sim \Lambda_{\text{QCD}}$. The correlator of these Wilson lines $1/N_c \text{Re}[\text{Tr}(V^\dagger(0)V(\mathbf{x}_\perp))]$ for two nuclei at different energies is shown in Fig. 4 (middle and right). The scale of the fluctuations of this quantity is $1/Q_s(\mathbf{x}_\perp)$, which is smaller for the higher energy case (right).

6. For each nucleus an $SU(N_c)$ matrix V_j is assigned at each lattice site j . They define a pure gauge configuration with the link variables

$$U_j^i = V_j V_{j+\hat{e}_i}^\dagger, \quad (17)$$

where $+\hat{e}_i$ indicates a shift from j by one lattice site in the $i = 1, 2$ direction.

7. The Wilson lines in the future light-cone U_j^i are determined from those of the two nuclei (A and B) by solving

$$\text{tr} \left\{ t^a \left[\left(U_{(A)}^i + U_{(B)}^i \right) (1 + U^{i\dagger}) - (1 + U^i) \left(U_{(A)}^{i\dagger} + U_{(B)}^{i\dagger} \right) \right] \right\} = 0 \quad (18)$$

iteratively [40]. Here t^a are the generators of $SU(3)$ in the fundamental representation.

8. The lattice expression for the longitudinal electric field can then be obtained from the solutions U^i and $U_{(A,B)}^i$ [40].

9. Given these initial conditions, the source free Yang-Mills equations are solved forward in time (see Section II B).

From the boost invariant gauge field configurations at finite times one can determine the gluon multiplicity and the energy momentum tensor as a function of transverse position. Employing the proper impact parameter distribution [21] obtained from the Glauber model, the gluon multiplicity distribution can be computed in transverse Coulomb gauge $\partial_i A^i = 0$, $i = 1, 2$, and compared to the measured charged hadron multiplicity distribution. The result for RHIC energies comparing to uncorrected data from the STAR collaboration is shown in Fig. 5. It was shown [60] that gluons produced from the Glasma naturally follow negative binomial distributions. This can be seen from the distributions for small impact parameter ranges in Fig. 5. It was demonstrated in [20] that these distributions are indeed fit best by negative binomial distributions.

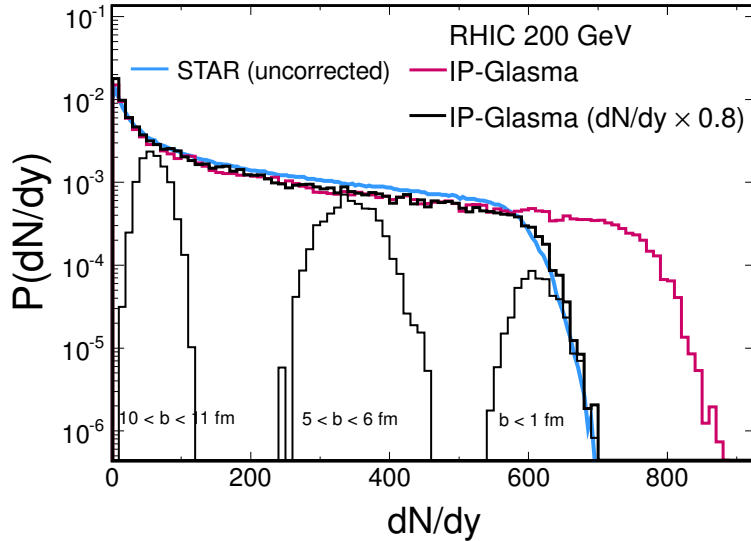


FIG. 5: Gluon multiplicity distribution. Shown are also distributions for limited ranges of impact parameter b . Experimental data from STAR [61]. Figure from [21].

D. Connection to hydrodynamics and comparison to data

We now discuss how the classical color fields from the IP-Glasma calculation are translated into an initial condition for hydrodynamics, and show comparisons with experimental data for several observables.

The main equations of hydrodynamics are energy and momentum conservation $\partial_\mu T^{\mu\nu} = 0$ along with an equation of state, where $T^{\mu\nu}$ is the energy momentum tensor. They need to be supplemented by an initial condition for $T^{\mu\nu}$ at some early time, often called the “thermalization time”. The IP-Glasma model provides the gauge field $T^{\mu\nu}$ with one caveat: the gluon field configurations of the IP-Glasma model are not in local equilibrium. In fact, when

switching from IP-Glasma dynamics to hydrodynamics at a time of $0.2 \text{ fm}/c$, the longitudinal pressure of the fields is approximately zero, and negative at earlier times. We will discuss the possibility to reach equilibrium in the Yang-Mills system when including quantum corrections and considering fully three dimensional dynamics below. Lacking a mechanism for equilibration in the 2+1 dimensional LO theory, one way to provide an initial condition for the hydrodynamic equations is to neglect the non-equilibrium components of $T^{\mu\nu}$ and extract the energy density and initial flow velocities by solving the identity $u_\mu T^{\mu\nu} = \varepsilon u^\nu$ [22]. There will be discontinuities in other components of $T^{\mu\nu}$ as one switches from the anisotropic field energy momentum tensor to the equilibrium one, which contains the isotropic pressure obtained from the equation of state. However, this should be a good first approximation for matching to fluid dynamics.

Here we will review results for observables that are sensitive to the fluctuations in the initial state of the collision. We will demonstrate that the IP-Glasma model produces fluctuating initial geometries that are consistent with the flow harmonics v_n and their event-by-event fluctuations measured at the LHC.

The v_n are the coefficients in a Fourier expansion of the azimuthal charged hadron distribution, which is obtained after evolving the hydrodynamic medium and performing a “freeze-out” wherever the system reaches a given minimal temperature or energy density. Every cell, which reaches that threshold, will act like a black body radiator of thermally distributed particles [62]. Resonances then decay according to the experimentally observed branching ratios, resulting in the final particle distributions.

1. Flow harmonics v_n

Fluid dynamics translates initial geometries into momentum anisotropies, which are quantified by the v_n . Thus, apart from the right transport properties, a theoretical description must contain the correct initial geometry including event-by-event fluctuations. Fluctuations have a significant effect even on the average values of the v_n , most notably for odd n : Without fluctuating initial conditions the odd harmonics would be zero by symmetry.

The IP-Glasma model in combination with viscous fluid dynamics described above has been shown to lead to an exceptionally good description of all flow harmonics, both as functions of transverse momentum and collision centrality [22]. This is a non-trivial result because other initial state models could not describe v_2 and v_3 simultaneously [63]. In Fig. 6 we show v_n ($n = 2, \dots, 5$) as functions of p_\perp and centrality for Pb+Pb collisions at LHC with a center of mass energy of $\sqrt{s} = 2.76 \text{ TeV}$.

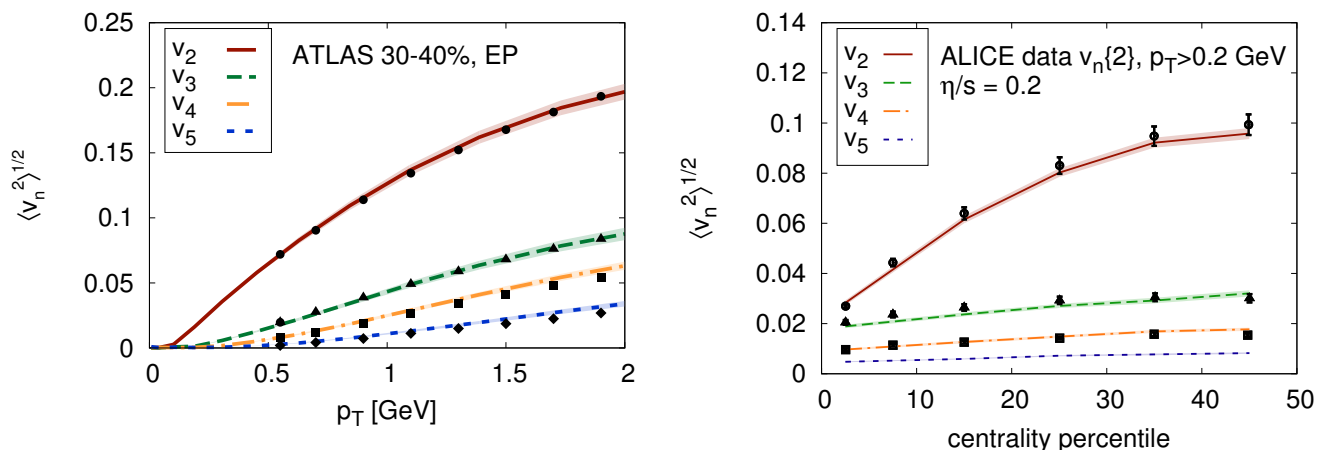


FIG. 6: Left: Transverse momentum dependent rms v_n compared to ATLAS data [64]. Right: Centrality dependent rms v_n compared to ALICE data [65]. Figure adapted from [22].

2. v_n distributions

An observable that is particularly sensitive to the initial state fluctuations but almost insensitive to the transport properties of the medium is the event-by-event distribution of harmonic flow coefficients [18, 19, 22]. As discussed in the introduction, several initial state models could be excluded by comparing their predictions for the event-by-event elliptic flow distributions in different centrality classes with experimental data [19].

Calculations of scaled event-by-event v_n distributions using the IP-Glasma model combined with hydrodynamic evolution are in exceptional agreement with experimental data [22, 66]. This is demonstrated for 20-25% central events in Fig. 7. For not too peripheral events or too large harmonic number n the initial eccentricity distributions already yield a very good description of the experimental data. These results indicate that the initial state fluctuations

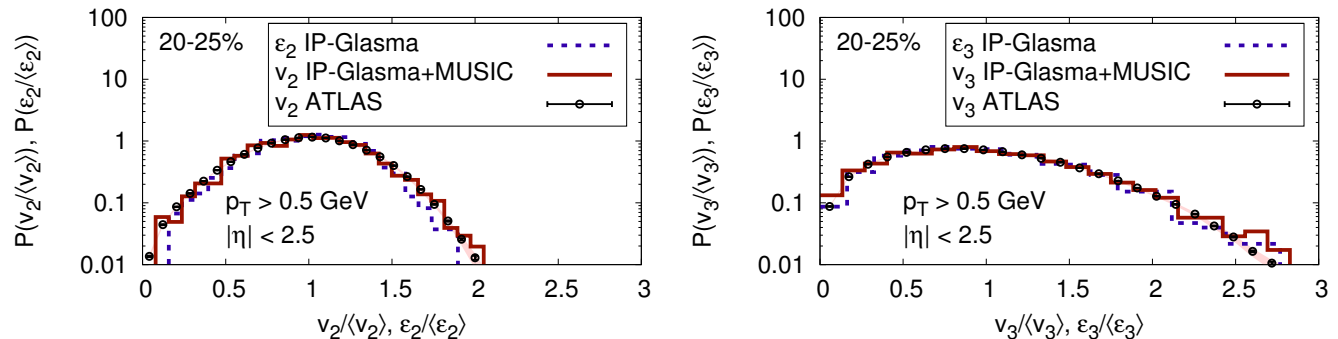


FIG. 7: Event-by-event distributions of elliptic (left) and triangular (right) flow coefficients in $\sqrt{s} = 2.76$ TeV collisions at LHC, scaled by the mean values and compared to ATLAS data [18]. Also shown are the scaled initial state eccentricity distributions.

used in the IP-Glasma model describe the experimental reality very well.

3. Shape-multiplicity correlations in $U+U$ collisions

Another observable that is sensitive to fluctuations and the mechanism of particle production and able to exclude initial state models is the correlation between multiplicity and elliptic flow in ultra-central collisions of deformed nuclei such as uranium U [67]. A Glauber model in which the multiplicity has a significant contribution proportional to the number of binary collisions N_{bin} predicts a strong anti-correlation between v_2 and the multiplicity in ultra-central $U+U$ collisions. This is because N_{bin} is much larger in the case that the longer axes of both nuclei are aligned with the beam line, than if the shorter axes are.

In contrast, along with a simple constituent quark model, the IP-Glasma model predicts a weaker anti-correlation of the initial geometry with the multiplicity [68], which is very close to the experimental data as demonstrated in Fig. 8.

In the IP-Glasma model the multiplicity is proportional to $Q_s^2 S_{\perp} / \alpha_s(Q_2)$ where S_{\perp} is the transverse size of the overlap region. For tip-tip collisions, which have the smallest v_2 , the increase in Q_s^2 is balanced by a decrease in S_{\perp} . α_s decreases only logarithmically with increasing Q_s^2 leading to a mildly increased multiplicity in tip-tip collisions compared to body-body collisions (which have the largest v_2 due to the prolate shape of the U nucleus). The data indicate that effects from sub-nucleonic structure and coherence, as included in the IP-Glasma model, are present and important [67].

III. QUANTUM FLUCTUATIONS

A. General considerations

The CGC at LO already contains fluctuations of the positions of the nucleons inside a nucleus, and of the distribution of the color charges inside a nucleon. But once the nucleon positions and the color distribution in each nucleon has been chosen, the outcome is deterministic.

At next-to-leading order (NLO), new fluctuations –of quantum origin– appear and the fields are no longer determined deterministically from the color sources. These quantum fluctuations can a priori be of two kinds:

- i. Initial state fluctuations.** Because of the uncertainty principle, the fields and their conjugate momenta cannot be known with arbitrary accuracy. Therefore, a *quantum* initial state must have fluctuations of the initial values of the fields, in contrast with the CGC at LO. The minimal variance of these fluctuations is controlled by Planck's constant \hbar .

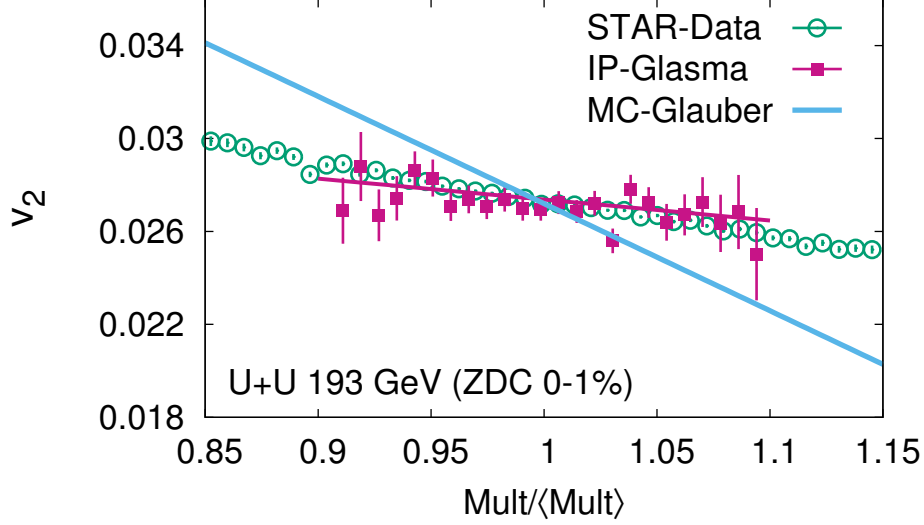


FIG. 8: Correlation between v_2 ($\varepsilon_2 \langle v_2 \rangle / \langle \varepsilon_2 \rangle$ in the theoretical curves) and the scaled multiplicity in 0-1% central U+U events at $\sqrt{s} = 193$ GeV. The magenta line is a fit to the IP-Glasma result. Experimental data from STAR [67].

ii. Quantum “jumps” in the time evolution. In contrast with the LO where Hamilton equations provide unique time derivatives of the fields from their current values, quantum fluctuations also make the evolution non deterministic.

However, NLO corrections (one-loop) are rather special because they only contain quantum fluctuations from the initial state (beyond NLO, fluctuations are both in the initial state and in the evolution). In a quantum system whose classical phase-space is described by coordinates \mathbf{X} and by momenta \mathbf{P} , the density matrix ρ_t evolves according to

$$\partial_t \rho_t = i[H, \rho_t], \quad (19)$$

where H is the Hamiltonian operator. A completely equivalent representation is obtained by introducing the *Wigner representation*,

$$\begin{aligned} \mathcal{W}_t(\mathbf{X}, \mathbf{P}) &\equiv \int d\mathbf{s} e^{\frac{i}{\hbar} \mathbf{P} \cdot \mathbf{s}} \langle \mathbf{X} - \frac{\mathbf{s}}{2} | \rho_t | \mathbf{X} + \frac{\mathbf{s}}{2} \rangle \\ \mathcal{H}(\mathbf{X}, \mathbf{P}) &\equiv \int d\mathbf{s} e^{\frac{i}{\hbar} \mathbf{P} \cdot \mathbf{s}} \langle \mathbf{X} - \frac{\mathbf{s}}{2} | H | \mathbf{X} + \frac{\mathbf{s}}{2} \rangle. \end{aligned} \quad (20)$$

Note that \mathbf{X} and \mathbf{P} are commuting classical coordinates, not quantum operators. \mathcal{W}_t is called the Wigner distribution, and \mathcal{H} is the classical Hamiltonian. \mathcal{W}_t evolves as

$$\begin{aligned} \partial_t \mathcal{W}_t(\mathbf{X}, \mathbf{P}) &= \frac{2}{\hbar} \mathcal{H}(\mathbf{X}, \mathbf{P}) \sin \left(\frac{\hbar}{2} \left(\overleftarrow{\nabla}_{\mathbf{X}} \overrightarrow{\nabla}_{\mathbf{P}} - \overleftarrow{\nabla}_{\mathbf{P}} \overrightarrow{\nabla}_{\mathbf{X}} \right) \right) \mathcal{W}_t(\mathbf{X}, \mathbf{P}) \\ &\underset{\hbar \rightarrow 0}{\approx} \underbrace{\{\mathcal{H}, \mathcal{W}_t\}}_{\text{Poisson bracket}} + \mathcal{O}(\hbar^2). \end{aligned} \quad (21)$$

The first line is exact, and the second line shows the lowest order in \hbar . At the order \hbar^0 , we recover classical Hamiltonian dynamics, in the form of the Liouville equation. Remarkably, the first correction arises only at the \hbar^2 level: at the order \hbar^1 , the time evolution remains classical, and the only quantum effects come from the initial state.

B. One loop corrections

Consider now the 1-loop corrections to an observable $\mathcal{O}(A, \partial A, \dots)$, that depends on the gauge field operator and its derivatives. One must evaluate graphs such as the one shown in Fig. 2, that contain a loop embedded in the LO

classical field [69, 70]. When its *endpoints have a space-like separation*³, the gluon propagator in a background field reads [72]:

$$\mathcal{G}^{\mu a, \nu b}(x, y) \stackrel{=}{(x-y)^2 \leq 0} \sum_{\lambda, c} \int \frac{d^3 \mathbf{k}}{(2\pi)^3 2|\mathbf{k}|} a_{\mathbf{k}\lambda c}^{\mu a}(x) a_{\mathbf{k}\lambda c}^{\nu b*}(y), \quad (22)$$

where $a_{\mathbf{k}\lambda c}^{\mu a}(x)$ is a small perturbation obeying the *linearized* Yang-Mills equations about the classical field \mathcal{A}^μ ,

$$[\mathcal{D}_\mu, [\mathcal{D}^\mu, a^\nu] - [\mathcal{D}^\nu, a^\mu]] - ig [\mathcal{F}^{\nu\mu}, a_\mu] = 0, \quad \lim_{t \rightarrow -\infty} a_{\mathbf{k}\lambda c}^{\mu a}(x) = \epsilon_{\mathbf{k}\lambda}^\mu \delta_c^a e^{ik \cdot x}. \quad (23)$$

\mathcal{D}_μ and $\mathcal{F}^{\mu\nu}$ are the covariant derivative and field strength constructed with the classical field \mathcal{A}^μ . Eq. (22) can also be written as a Gaussian average over random fields,

$$\mathcal{G}^{\mu a, \nu b}(x, y) \stackrel{=}{(x-y)^2 \leq 0} \langle A^{\mu a}(x) A^{\nu b}(y) \rangle \quad (24)$$

with

$$A^{\mu a}(x) \equiv \sum_{\lambda, c} \int \frac{d^3 \mathbf{k}}{(2\pi)^3 2|\mathbf{k}|} \left[c_{\mathbf{k}\lambda c} a_{\mathbf{k}\lambda c}^{\mu a}(x) + \text{c.c.} \right],$$

$$\langle c_{\mathbf{k}\lambda c} \rangle = 0, \quad \langle c_{\mathbf{k}\lambda c} c_{\mathbf{k}'\lambda'c'}^* \rangle = \frac{1}{2} 2|\mathbf{k}| (2\pi)^3 \delta(\mathbf{k} - \mathbf{k}') \delta_{\lambda\lambda'} \delta_{cc'}. \quad (25)$$

The fields $A^{\mu a}$ in Eq. (24) are linear superpositions of the $a_{\mathbf{k}\lambda c}$ with random coefficients that are a classical analogue of creation and annihilation operators. Their variance in Eq. (25) indicates that they correspond to an occupation number 1/2, that can be interpreted as the zero-point quantum fluctuations in each mode.

Using Eq. (22), the NLO correction to an inclusive observable can be written as follows:

$$\langle \mathcal{O} \rangle_{\text{NLO}} = \left[\frac{1}{2} \int \int_{\mathbf{k}} [a_{\mathbf{k}} \mathbb{T}]_{\mathbf{u}} [a_{\mathbf{k}}^* \mathbb{T}]_{\mathbf{v}} + \int_{\mathbf{u} \in \Sigma} [\boldsymbol{\alpha} \mathbb{T}]_{\mathbf{u}} \right] \langle \mathcal{O} \rangle_{\text{LO}}. \quad (26)$$

In this formula, $\langle \mathcal{O} \rangle_{\text{LO}}$ depends on the classical field \mathcal{A}^μ on a surface Σ , where the initial value of the classical field is specified, e.g. a surface $\tau = \text{const.}$ $\mathbb{T}_{\mathbf{u}}$ is the generator of shifts of this initial field: for any function $\mathcal{F}[\mathcal{A}_\Sigma]$ of the fields on Σ , we have

$$\left[\exp \int_{\mathbf{u} \in \Sigma} [\boldsymbol{\alpha} \mathbb{T}]_{\mathbf{u}} \right] \mathcal{F}[\mathcal{A}_\Sigma] = \mathcal{F}[\mathcal{A}_\Sigma + \boldsymbol{\alpha}]. \quad (27)$$

The functions $a_{\mathbf{k}}$ in Eq. (26) are the mode functions introduced in Eq. (22) and the function $\boldsymbol{\alpha}$ can also be expressed in terms of the same mode functions. Eq. (26) shows that the NLO can be obtained from the LO by fiddling with the initial values of the classical fields, while the fields continue to evolve classically. Note that formulas such as (26) cannot be exact at 2-loops [73].

C. Boost invariant fluctuations and factorization

Some of these fluctuations leads to logarithms of the cutoff that separates the sources from the field degrees of freedom [72, 74, 75]. One can prove that

$$\begin{aligned} \frac{1}{2} \int \int_{\mathbf{k}} [a_{\mathbf{k}} \mathbb{T}]_{\mathbf{u}} [a_{\mathbf{k}}^* \mathbb{T}]_{\mathbf{v}} + \int_{\mathbf{u} \in \Sigma} [\boldsymbol{\alpha} \mathbb{T}]_{\mathbf{u}} &= \\ &= \log(\Lambda^+) \mathcal{H}_1 + \log(\Lambda^-) \mathcal{H}_2 + \text{terms w/o logs}, \end{aligned} \quad (28)$$

³ For time-like separations, the propagator receives extra contributions that depend on the time ordering [71].

where the operators $\mathcal{H}_{1,2}$ are the *JIMWLK Hamiltonians* of the projectiles [76]. The fluctuations that give logarithms of Λ^+ (resp. Λ^-) have a large momentum rapidity in the direction of the nucleus 1 (resp. nucleus 2). To the observer, these field fluctuations appear as fast moving color charges, similar the degrees of freedom already included in $\rho_{1,2}$.

Eq. (28) substantiates this intuitive picture. It implies that these logarithms can be absorbed into redefinitions of the distributions $W[\rho_{1,2}]$, evolving with the cutoff according to ([76–84], see also [85–91] for next-to-leading log corrections)

$$\frac{\partial W}{\partial \Lambda} = -\mathcal{H} W. \quad (29)$$

This works because Eq. (28) does not mix ρ_1 and ρ_2 , a consequence of *causality*: the logarithms come from soft radiation by fast color charges, which has a long formation time and must occur long before the collision. Therefore, the radiation in nuclei 1 and 2 are independent. All the fluctuation modes that have a rapidity separation $\Delta y \gtrsim \alpha_s^{-1}$ with the observer can be resummed in this way, leading to a factorized expression

$$\langle \mathcal{O} \rangle_{\text{Leading Log}} = \int [D\rho_1] [D\rho_2] W_1[\rho_1] W_2[\rho_2] \mathcal{O}_{\text{LO}}(\rho_{1,2}), \quad (30)$$

where W_1 and W_2 are solutions of Eq. (29), starting from an initial condition at the rapidity of the projectile and evolving to the rapidity of the observer. In this new light, the Gaussian distribution introduced in Eq. (2) should be viewed as a model for the initial color distribution, but non-Gaussian correlations may develop when evolving away from the projectile.

Thanks to its structure, the JIMWLK Hamiltonian can be interpreted as a diffusion operator in a functional space, which allows to reproduce the rapidity evolution of $W[\rho]$ by a random walk described by a Langevin equation [92]. This approach has been used in several works addressing the numerical study of the JIMWLK equation [93, 94]. Note also that, for simple correlators of color charges, this evolution is well described by a mean field approximation known as the *Balitsky-Kovchegov equation* [95] (see [85, 96–98] for next-to-leading log corrections).

D. Rapidity dependent fluctuations

The fluctuation modes that give logarithms in Eq. (28) preserve the η -independence of the LO. The remaining modes are η -dependent, but do not give large logarithms. It is convenient to introduce a new basis:

$$b_{\mathbf{k}_\perp \nu \lambda c}^{\mu a} \equiv \int dy e^{i\nu y} a_{\mathbf{k}_\perp k_z \lambda c}^{\mu a}, \quad (31)$$

where y is the momentum rapidity $y = \ln((k_0 + k_z)/(k_0 - k_z))/2$. Since the $a_{\mathbf{k} \lambda c}(\mathbf{x})$ depend on the momentum and spacetime rapidities only via the difference $y - \eta$, $b_{\mathbf{k}_\perp \nu \lambda c}$ has a trivial rapidity dependence in $\exp(i\nu\eta)$.

The mode functions $b_{\mathbf{k} \lambda c}$ can be calculated analytically up to a proper time $Q_s \tau \ll 1$ [99] (beyond this time, the classical background field itself is not known analytically), in $A^\tau = 0$ gauge:

$$\begin{aligned} b_{\mathbf{k}_\perp \nu \lambda c}^{ia}(\tau, \eta, \mathbf{x}) &= F_{\mathbf{k}_\perp \nu \lambda c}^{+,ia}(\tau, \eta, \mathbf{x}) + F_{\mathbf{k}_\perp \nu \lambda c}^{-,ia}(\tau, \eta, \mathbf{x}) \\ b_{\mathbf{k}_\perp \nu \lambda c}^{\eta a}(\tau, \eta, \mathbf{x}) &= \mathcal{D}_{ab}^i \left(\frac{F_{\mathbf{k}_\perp \nu \lambda c}^{+,ib}(\tau, \eta, \mathbf{x})}{2 + i\nu} - \frac{F_{\mathbf{k}_\perp \nu \lambda c}^{-,ib}(\tau, \eta, \mathbf{x})}{2 - i\nu} \right), \end{aligned} \quad (32)$$

where we denote

$$\begin{aligned} F_{\mathbf{k}_\perp \nu \lambda c}^{+,ia}(\tau, \eta, \mathbf{x}) &\equiv \Gamma(-i\nu) e^{+\frac{\nu\pi}{2}} e^{i\nu\eta} V_{1ab}^\dagger(\mathbf{x}) \vartheta_\lambda^j \\ &\times \int \frac{d^2 \mathbf{p}_\perp}{(2\pi)^2} e^{i\mathbf{p} \cdot \mathbf{x}} \tilde{V}_{1bc}(\mathbf{p} + \mathbf{k}_\perp) \left(\frac{p_\perp^2 \tau}{2k_\perp} \right)^{+i\nu} \left[\delta^{ji} - \frac{2p_\perp^j p_\perp^i}{p_\perp^2} \right] \\ F_{\mathbf{k}_\perp \nu \lambda c}^{-,ia}(\tau, \eta, \mathbf{x}) &\equiv \Gamma(+i\nu) e^{-\frac{\nu\pi}{2}} e^{i\nu\eta} V_{2ab}^\dagger(\mathbf{x}) \vartheta_{k\lambda}^j \\ &\times \int \frac{d^2 \mathbf{p}_\perp}{(2\pi)^2} e^{i\mathbf{p} \cdot \mathbf{x}} \tilde{V}_{2bc}(\mathbf{p} + \mathbf{k}_\perp) \left(\frac{p_\perp^2 \tau}{2k_\perp} \right)^{-i\nu} \left[\delta^{ji} - \frac{2p_\perp^j p_\perp^i}{p_\perp^2} \right] \end{aligned} \quad (33)$$

and $\vartheta_{\mathbf{k}\lambda}^i \equiv (\delta^{ij} - 2 \frac{k^i k^j}{k_\perp^2}) \epsilon_{\mathbf{k}\lambda}^j$. The Wilson lines $V_{1,2}$ have been introduced in Eq. (11) (here, they are in the adjoint representation), and the covariant derivative \mathcal{D}_{ab}^i is constructed from the initial field A_0^i given in Eq. (10). The corresponding electrical fields are obtained by time derivatives of Eqs. (32). Since these expressions are only valid at very short proper times, they should be used as initial conditions for Eq. (23).

E. Instabilities and classical statistical approximation

After having resummed the large logarithms via the JIMWLK evolution, the remaining contributions are seemingly suppressed by a factor α_s compared to LO. However, this conclusion is invalidated by the chaotic behavior of classical solutions of Yang-Mills equations⁴, that are exponentially sensitive to their initial conditions [102–112]. Consequently, some of the mode functions $a_{\mathbf{k}\lambda c}$ grow exponentially with time, and the NLO corrections contain exponentially growing terms: the suppression factor α_s quickly becomes irrelevant in view of this time dependence.

The fastest growing can be summed to all orders by exponentiating the quadratic part of the operator that appears in Eq. (26), giving an expression that depends on classical fields averaged over a Gaussian ensemble of fluctuating initial conditions [70]. This approximation is known as *classical statistical approximation* (CSA). A strict application of this scheme leads to initial fields that are the sum of the LO classical field \mathcal{A}^μ (non fluctuating), and a fluctuating part given by Eq. (25) [113]:

$$A^{\mu a}(x) = \mathcal{A}^{\mu a}(x) + \sum_{\lambda, c} \int \frac{d^3 \mathbf{k}}{(2\pi)^3 2|\mathbf{k}|} \left[c_{\mathbf{k}\lambda c} a_{\mathbf{k}\lambda c}^{\mu a}(x) + \text{c.c.} \right],$$

$$\langle c_{\mathbf{k}\lambda c} \rangle = 0, \quad \langle c_{\mathbf{k}\lambda c} c_{\mathbf{k}'\lambda' c'}^* \rangle = \frac{1}{2} 2|\mathbf{k}| (2\pi)^3 \delta(\mathbf{k} - \mathbf{k}') \delta_{\lambda\lambda'} \delta_{cc'}. \quad (34)$$

However, such a spectrum of fluctuations combined with classical time evolution leads to results that are very sensitive to the ultraviolet cutoff [114]. More formally, this resummation breaks the renormalizability of the underlying theory [115, 116].

A variant of the CSA uses as initial condition the ensemble of fields corresponding to a classical gas of gluons with a distribution $f(\mathbf{k})$. Such initial fields have no non-fluctuating part, and the variance of the random coefficients is proportional to $f(\mathbf{k})$ [117–119]:

$$A^{\mu a}(x) = \sum_{\lambda, c} \int \frac{d^3 \mathbf{k}}{(2\pi)^3 2|\mathbf{k}|} \left[c_{\mathbf{k}\lambda c} a_{\mathbf{k}\lambda c}^{\mu a}(x) + \text{c.c.} \right],$$

$$\langle c_{\mathbf{k}\lambda c} \rangle = 0, \quad \langle c_{\mathbf{k}\lambda c} c_{\mathbf{k}'\lambda' c'}^* \rangle = f(\mathbf{k}) 2|\mathbf{k}| (2\pi)^3 \delta(\mathbf{k} - \mathbf{k}') \delta_{\lambda\lambda'} \delta_{cc'}. \quad (35)$$

If $f(\mathbf{k})$ decreases sufficiently fast, this modification leads to ultraviolet finite results.

F. Quantum fluctuations in kinetic theory

Eqs. (34) and (35) describe very different systems, despite their similarity:

- The flat spectrum of Eq. (34) on top of a classical field describes a quantum coherent state.
- The compact spectrum of Eq. (35) describes an incoherent classical state (quantum mechanics imposes a minimal variance $1/2$ in all modes).

When applied to simulations of the early stages of heavy ion collisions, these two types of fluctuating initial conditions lead to quite different behaviors of the pressure tensor.

In order to clarify the situation, it would be highly desirable to include quantum fluctuations without sacrificing renormalizability. In field theory, a framework that achieves this is the *2-particle irreducible* approximation [120–124] of the Kadanoff-Baym equations [125]. Although in principle feasible even for the expanding geometry encountered in heavy ion collisions [126, 127], this is much more complicated to implement than the CSA.

A simpler alternative is to study quantum fluctuations in kinetic theory. Schematically, the Boltzmann equation for $2 \rightarrow 2$ scatterings reads:

$$\partial_t f_3 \sim g^4 \int_{124} \cdots [f_1 f_2 (f_3 + f_4) - f_3 f_4 (f_1 + f_2)]$$

$$+ g^4 \int_{124} \cdots [f_1 f_2 - f_3 f_4]. \quad (36)$$

⁴ These instabilities are related to the Weibel instability that happens in anisotropic plasmas [100, 101].

where the dots encapsulates the cross-section and the delta functions for energy-momentum conservation, whose details are irrelevant here. In Eq. (36), we have written on the first line the terms that correspond to the classical approximation of Eq. (35), and on the second line the terms that come from quantum fluctuations.

Keeping only the cubic terms of the first line may be justified when the occupation number is large. However, this approximation is not uniform over all momentum space, which may be especially problematic in systems with an anisotropic momentum distribution. In the left part of Fig. 9, we illustrate this for a distribution nearly proportional

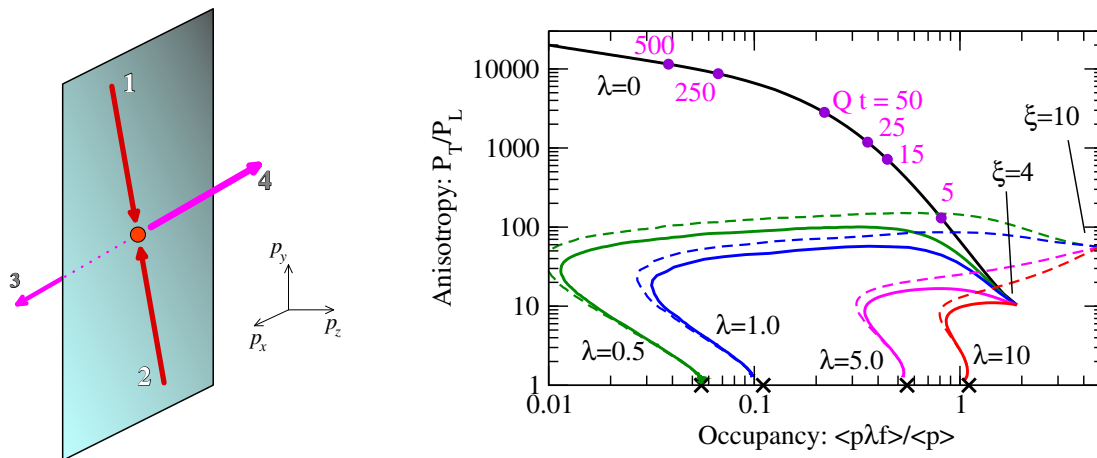


FIG. 9: Left: $2 \rightarrow 2$ scattering contributing to isotropization. Right: time evolution of the anisotropy with the classical ($\lambda = 0$) and complete ($\lambda = 0.5$ to 10) Boltzmann equations (plot taken from [33], with time labels added by us for clarity).

to $\delta(p_z)$, for which the incoming particles 1,2 have purely transverse momenta. Isotropization requires that at least one of the outgoing particles (3 or 4) has a nonzero p_z . Nonzero contributions with this kinematics can only come from the second line, which is dropped in the classical approximation.

This has been seen in numerical studies of the Boltzmann equation for a longitudinally expanding system [33, 128]. The right part of Fig.9 shows results with (curves $\lambda = 0.5$ to 10) and without (curve $\lambda = 0$) the terms of the second line. Starting at the time $Q\tau = 1$ from identical CGC-like initial conditions, the classical and quantum evolutions starts diverging around $Q\tau \approx 2$ for $\lambda = 0.5$ (i.e. $\alpha_s \approx 0.02$ for $N_c = 2$ colors), well before the conjectured range of validity of the classical approximation, $Q\tau \approx \alpha_s^{-3/2} \approx 350$. These considerations show that quantum fluctuations are essential for isotropization: purely classical approximations do not capture the relevant physics and fail at assessing their own range of validity.

IV. FLUCTUATIONS IN SMALL SYSTEMS, PROTON SHAPE

Proton-nucleus collisions, which were initially thought to be an easy to understand reference for heavy ion collisions, have lead to a number of new puzzles since a lot of the collectivity that appears in bigger systems is also visible there. While in nucleus-nucleus collisions, the fluctuations that are internal to a nucleon do not play a big role, because they are averaged over many nucleons, they may become crucial in proton-nucleus collisions.

The fluctuating geometry of a proton will most affect final observables such as anisotropy coefficients v_n if final state collective effects are dominant. Hydrodynamic calculations using fluctuating Monte Carlo Glauber initial conditions agree with a variety of experimental observables [66, 129–135]. However, more sophisticated models such as the IP-Glasma could not describe the measured v_2 and v_3 coefficients in p+Pb collisions [66]. The reason for this disagreement was the assumption of a round proton, which was not important for heavy ion collisions. However, in small systems additional sub-nucleonic fluctuations can make a significant difference. For example, the initial color charges in a proton could be concentrated around three valence quarks. It was shown in [136] that a proton will retain a memory of the fluctuating shape at large x after JIMWLK evolution over several units in rapidity. This means that a proton at high energy can have fluctuations on various length scales, not just $1/Q_s$.

An issue with the use of hydrodynamics in small systems is the possible break-down of its applicability. For small systems the Knudsen number, the ratio of a typical microscopic over a macroscopic scale, can become large, indicating that the hydrodynamic framework is beginning to break down [137]. However, this does not preclude the existence of final state effects, which could be described within a framework other than hydrodynamics.

Apart from the possibility that final state collective effects are dominant also in small collision systems, like p+A, initial state correlations that affect particle production can also contribute to the measured anisotropies [138–142]. In particular, the classical Yang Mills framework, which is the basis for the IP-Glasma model, contains multi gluon correlations that show qualitatively similar features as the experimental data, namely a relatively large v_2 and v_3 in p+A collisions [143]. Such effects would naturally lead to the observed long range rapidity correlations, which have to be assumed in most hydrodynamic calculations.

At this point it is not yet settled which of the two distinct effects described above dominates the creation of the observed anisotropies. A detailed discussion on the current status of the field can be found in [144]. Here we conclude that in either case the detailed understanding of sub-nucleonic fluctuations in the initial state is essential for the interpretation of the experimental data of multi particle correlations in small collision systems.

V. CONCLUSIONS

Fluctuations play a very important role at various levels in the description of heavy ion collisions. Phenomenologically, fluctuations are very important in obtaining the correct final state azimuthal correlations. Their effect is comparatively larger in collisions involving smaller observables, and it is still an open question whether the azimuthal patterns observed in the collision of small systems (p-p collisions) are mostly due to initial state quantum fluctuations.

On a more theoretical level, quantum fluctuations also seem essential in explaining the isotropization of the pressure tensor and the early applicability of hydrodynamics. The complete description of the early time dynamics and transition to the hydrodynamic regime is still an active field of research. Likely the full answer will involve various stages including the unstable evolution in classical Yang-Mills dynamics with quantum corrections and kinetic theory.

Acknowledgements

This manuscript has been accepted by Annual Reviews of Nuclear and Particle Science. FG is supported by the Agence Nationale de la Recherche project 11-BS04-015-01. BPS is supported by the US Department of Energy under DOE Contract No. DE-SC0012704.

-
- [1] T. Hirano and K. Tsuda, Phys. Rev. **C66**, 054905 (2002).
 - [2] P. F. Kolb and U. W. Heinz, Quark Gluon Plasma 3 ed R C Hwa and X N Wang (Singapore: World Scientific) p. 634 (2003), nucl-th/0305084.
 - [3] P. Huovinen, Quark Gluon Plasma 3 ed R C Hwa and X N Wang (Singapore: World Scientific) p. 600 (2003), nucl-th/0305064.
 - [4] P. Romatschke and U. Romatschke, Phys. Rev. Lett. **99**, 172301 (2007).
 - [5] G. Policastro, D. T. Son, and A. O. Starinets, Phys. Rev. Lett. **87**, 081601 (2001), hep-th/0104066.
 - [6] P. Kovtun et al., Phys. Rev. Lett. **94**, 111601 (2005).
 - [7] B. Schenke, S. Jeon, and C. Gale, Phys. Rev. Lett. **106**, 042301 (2011).
 - [8] P. Bozek and W. Broniowski, Phys. Rev. **C85**, 044910 (2012), 1203.1810.
 - [9] I. A. Karpenko, P. Huovinen, H. Petersen, and M. Bleicher, Phys. Rev. **C91**, 064901 (2015).
 - [10] U. Heinz and R. Snellings, Ann. Rev. Nucl. Part. Sci. **63**, 123 (2013), 1301.2826.
 - [11] C. Gale, S. Jeon, and B. Schenke, Int. J. Mod. Phys. **A28**, 1340011 (2013), 1301.5893.
 - [12] R. D. de Souza, T. Koide, and T. Kodama (2015), 1506.03863.
 - [13] S. Jeon and U. Heinz, Int. J. Mod. Phys. **E24**, 1530010 (2015), 1503.03931.
 - [14] B. Alver et al. (PHOBOS), Phys. Rev. Lett. **98**, 242302 (2007), nucl-ex/0610037.
 - [15] A. P. Mishra, R. K. Mohapatra, P. S. Saumia, and A. M. Srivastava, Phys. Rev. **C77**, 064902 (2008), 0711.1323.
 - [16] B. Alver and G. Roland, Phys. Rev. **C81**, 054905 (2010).
 - [17] B. H. Alver, C. Gombaud, M. Luzum, and J.-Y. Ollitrault, Phys. Rev. **C82**, 034913 (2010).
 - [18] G. Aad et al. (ATLAS), JHEP **11**, 183 (2013), 1305.2942.
 - [19] H. Niemi, G. S. Denicol, H. Holopainen, and P. Huovinen, Phys. Rev. **C87**, 054901 (2013), 1212.1008.
 - [20] B. Schenke, P. Tribedy, and R. Venugopalan, Phys. Rev. Lett. **108**, 252301 (2012).
 - [21] B. Schenke, P. Tribedy, and R. Venugopalan, Phys. Rev. **C86**, 034908 (2012).
 - [22] C. Gale, S. Jeon, B. Schenke, P. Tribedy, and R. Venugopalan, Phys. Rev. Lett. **110**, 012302 (2013).
 - [23] H. Niemi, K. J. Eskola, and R. Paatelainen (2015), 1505.02677.
 - [24] J. S. Moreland, J. E. Bernhard, and S. A. Bass, Phys. Rev. **C92**, 011901 (2015), 1412.4708.
 - [25] M. Martinez and M. Strickland, Nucl. Phys. **A856**, 68 (2011), 1011.3056.

- [26] M. Martinez, R. Ryblewski, and M. Strickland, Phys. Rev. **C85**, 064913 (2012), 1204.1473.
- [27] W. Florkowski, R. Ryblewski, and M. Strickland, Nucl. Phys. **A916**, 249 (2013), 1304.0665.
- [28] D. Bazow, U. W. Heinz, and M. Strickland, Phys. Rev. **C90**, 054910 (2014), 1311.6720.
- [29] M. Strickland, Acta Phys. Polon. **B45**, 2355 (2014), 1410.5786.
- [30] L. Tinti, R. Ryblewski, W. Florkowski, and M. Strickland, Nucl. Phys. **A946**, 29 (2016), 1505.06456.
- [31] M. Nopoush, M. Strickland, R. Ryblewski, D. Bazow, U. Heinz, and M. Martinez, Phys. Rev. **C92**, 044912 (2015), 1506.05278.
- [32] M. P. Heller, R. A. Janik, and P. Witaszczyk, Phys. Rev. Lett. **108**, 201602 (2012), 1103.3452.
- [33] A. Kurkela and Y. Zhu, Phys. Rev. Lett. **115**, 182301 (2015), 1506.06647.
- [34] A. Deshpande, R. Ent, and R. Milner, CERN Cour. **49N9**, 13 (2009).
- [35] F. Gelis, E. Iancu, J. Jalilian-Marian, and R. Venugopalan, Ann. Rev. Nucl. Part. Sci. **60**, 463 (2010), 1002.0333.
- [36] L. D. McLerran and R. Venugopalan, Phys. Rev. **D49**, 2233 (1994).
- [37] L. D. McLerran and R. Venugopalan, Phys. Rev. **D49**, 3352 (1994).
- [38] Y. V. Kovchegov, Phys. Rev. **D54**, 5463 (1996), hep-ph/9605446.
- [39] A. Kovner, L. D. McLerran, and H. Weigert, Phys. Rev. **D52**, 6231 (1995), hep-ph/9502289.
- [40] A. Krasnitz and R. Venugopalan, Nucl. Phys. **B557**, 237 (1999), hep-ph/9809433.
- [41] A. Krasnitz and R. Venugopalan, Phys. Rev. Lett. **84**, 4309 (2000).
- [42] A. Krasnitz and R. Venugopalan, Phys. Rev. Lett. **86**, 1717 (2001).
- [43] A. Krasnitz, Y. Nara, and R. Venugopalan, Phys. Rev. Lett. **87**, 192302 (2001).
- [44] A. Krasnitz, Y. Nara, and R. Venugopalan, Nucl. Phys. **A727**, 427 (2003).
- [45] T. Lappi, Phys. Rev. **C67**, 054903 (2003).
- [46] T. Lappi, Phys. Lett. **B643**, 11 (2006).
- [47] A. Krasnitz, Y. Nara, and R. Venugopalan, Phys. Lett. **B554**, 21 (2003).
- [48] A. Krasnitz, Y. Nara, and R. Venugopalan, Nucl. Phys. **A717**, 268 (2003).
- [49] T. Lappi and R. Venugopalan, Phys. Rev. **C74**, 054905 (2006).
- [50] T. Lappi and L. McLerran, Nucl. Phys. **A772**, 200 (2006), hep-ph/0602189.
- [51] A. Dumitru, Y. Nara, and E. Petreska, Phys. Rev. **D88**, 054016 (2013), 1302.2064.
- [52] A. Dumitru, T. Lappi, and Y. Nara, Phys. Lett. **B734**, 7 (2014), 1401.4124.
- [53] J. Bartels, K. J. Golec-Biernat, and H. Kowalski, Phys. Rev. **D66**, 014001 (2002).
- [54] H. Kowalski and D. Teaney, Phys. Rev. **D68**, 114005 (2003).
- [55] H. Kowalski, T. Lappi, and R. Venugopalan, Phys. Rev. Lett. **100**, 022303 (2008).
- [56] H. Kowalski, L. Motyka, and G. Watt, Phys. Rev. **D74**, 074016 (2006).
- [57] B. Schenke, P. Tribedy, and R. Venugopalan, Phys. Rev. **C89**, 024901 (2014), 1311.3636.
- [58] A. H. Rezaeian, M. Siddikov, M. Van de Klundert, and R. Venugopalan, Phys. Rev. **D87**, 034002 (2013), 1212.2974.
- [59] T. Lappi, Eur. Phys. J. **C55**, 285 (2008).
- [60] F. Gelis, T. Lappi, and L. McLerran, Nucl. Phys. **A828**, 149 (2009).
- [61] B. I. Abelev et al. (STAR), Phys. Rev. **C79**, 034909 (2009), 0808.2041.
- [62] F. Cooper and G. Frye, Phys. Rev. **D10**, 186 (1974).
- [63] Z. Qiu, C. Shen, and U. W. Heinz, Phys. Lett. **B707**, 151 (2012).
- [64] G. Aad et al. (ATLAS Collaboration), Phys. Rev. **C86**, 014907 (2012).
- [65] K. Aamodt et al. (ALICE Collaboration), Phys. Rev. Lett. **107**, 032301 (2011).
- [66] B. Schenke and R. Venugopalan, Phys. Rev. Lett. **113**, 102301 (2014), 1405.3605.
- [67] L. Adamczyk et al. (STAR), Phys. Rev. Lett. **115**, 222301 (2015), 1505.07812.
- [68] B. Schenke, P. Tribedy, and R. Venugopalan, Phys. Rev. **C89**, 064908 (2014), 1403.2232.
- [69] F. Gelis and R. Venugopalan, Nucl. Phys. **A776**, 135 (2006), hep-ph/0601209.
- [70] F. Gelis, T. Lappi, and R. Venugopalan, Int. J. Mod. Phys. **E16**, 2595 (2007), 0708.0047.
- [71] T. Epelbaum and F. Gelis, Nucl. Phys. **A872**, 210 (2011), 1107.0668.
- [72] F. Gelis, T. Lappi, and R. Venugopalan, Phys. Rev. **D78**, 054019 (2008), 0804.2630.
- [73] F. Gelis and J. u. Laidet, Phys. Rev. **D87**, 045019 (2013), 1211.1191.
- [74] F. Gelis, T. Lappi, and R. Venugopalan, Phys. Rev. **D78**, 054020 (2008), 0807.1306.
- [75] F. Gelis, T. Lappi, and R. Venugopalan, Phys. Rev. **D79**, 094017 (2009), 0810.4829.
- [76] I. Balitsky, Nucl. Phys. **B463**, 99 (1996), hep-ph/9509348.
- [77] J. Jalilian-Marian, A. Kovner, L. D. McLerran, and H. Weigert, Phys. Rev. **D55**, 5414 (1997), hep-ph/9606337.
- [78] J. Jalilian-Marian, A. Kovner, A. Leonidov, and H. Weigert, Nucl. Phys. **B504**, 415 (1997), hep-ph/9701284.
- [79] J. Jalilian-Marian, A. Kovner, A. Leonidov, and H. Weigert, Phys. Rev. **D59**, 014014 (1998), hep-ph/9706377.
- [80] J. Jalilian-Marian, A. Kovner, and H. Weigert, Phys. Rev. **D59**, 014015 (1999), hep-ph/9709432.
- [81] J. Jalilian-Marian, A. Kovner, A. Leonidov, and H. Weigert, Phys. Rev. **D59**, 034007 (1999), [Erratum: Phys. Rev. **D59**, 099903 (1999)], hep-ph/9807462.
- [82] E. Iancu, A. Leonidov, and L. D. McLerran, Nucl. Phys. **A692**, 583 (2001), hep-ph/0011241.
- [83] E. Iancu, A. Leonidov, and L. D. McLerran, Phys. Lett. **B510**, 133 (2001), hep-ph/0102009.
- [84] E. Ferreira, E. Iancu, A. Leonidov, and L. McLerran, Nucl. Phys. **A703**, 489 (2002), hep-ph/0109115.
- [85] I. Balitsky and G. A. Chirilli, Phys. Rev. **D77**, 014019 (2008), 0710.4330.
- [86] I. Balitsky and G. A. Chirilli, Nucl. Phys. **B822**, 45 (2009), 0903.5326.
- [87] I. Balitsky and G. A. Chirilli, Phys. Rev. **D88**, 111501 (2013), 1309.7644.

- [88] A. V. Grabovsky, JHEP **09**, 141 (2013), 1307.5414.
- [89] A. Kovner, M. Lublinsky, and Y. Mulian, Phys. Rev. **D89**, 061704 (2014), 1310.0378.
- [90] A. Kovner, M. Lublinsky, and Y. Mulian, JHEP **04**, 030 (2014), 1401.0374.
- [91] A. Kovner, M. Lublinsky, and Y. Mulian, JHEP **08**, 114 (2014), 1405.0418.
- [92] J.-P. Blaizot, E. Iancu, and H. Weigert, Nucl. Phys. **A713**, 441 (2003), hep-ph/0206279.
- [93] K. Rummukainen and H. Weigert, Nucl. Phys. **A739**, 183 (2004), hep-ph/0309306.
- [94] A. Dumitru, J. Jalilian-Marian, T. Lappi, B. Schenke, and R. Venugopalan, Phys. Lett. **B706**, 219 (2011), 1108.4764.
- [95] Y. V. Kovchegov, Phys. Rev. **D60**, 034008 (1999), hep-ph/9901281.
- [96] I. Balitsky, Phys. Rev. **D75**, 014001 (2007), hep-ph/0609105.
- [97] Y. V. Kovchegov and H. Weigert, Nucl. Phys. **A784**, 188 (2007), hep-ph/0609090.
- [98] E. Gardi, J. Kuokkanen, K. Rummukainen, and H. Weigert, Nucl. Phys. **A784**, 282 (2007), hep-ph/0609087.
- [99] T. Epelbaum and F. Gelis, Phys. Rev. **D88**, 085015 (2013), 1307.1765.
- [100] S. Mrowczynski, Phys. Lett. **B314**, 118 (1993).
- [101] S. Mrowczynski, Phys. Lett. **B393**, 26 (1997), hep-ph/9606442.
- [102] T. S. Biro, C. Gong, B. Muller, and A. Trayanov, Int. J. Mod. Phys. **C5**, 113 (1994), nucl-th/9306002.
- [103] U. W. Heinz, C. R. Hu, S. Leupold, S. G. Matinyan, and B. Muller, Phys. Rev. **D55**, 2464 (1997), hep-th/9608181.
- [104] J. Bolte, B. Muller, and A. Schafer, Phys. Rev. **D61**, 054506 (2000), hep-lat/9906037.
- [105] P. Romatschke and R. Venugopalan, Phys. Rev. Lett. **96**, 062302 (2006), hep-ph/0510121.
- [106] P. Romatschke and R. Venugopalan, Eur. Phys. J. **A29**, 71 (2006), hep-ph/0510292.
- [107] P. Romatschke and R. Venugopalan, Phys. Rev. **D74**, 045011 (2006), hep-ph/0605045.
- [108] K. Fukushima, Phys. Rev. **C76**, 021902 (2007), [Erratum: Phys. Rev. **C77**, 029901 (2007)], 0711.2634.
- [109] H. Fujii and K. Itakura, Nucl. Phys. **A809**, 88 (2008), 0803.0410.
- [110] H. Fujii, K. Itakura, and A. Iwazaki, Nucl. Phys. **A828**, 178 (2009), 0903.2930.
- [111] T. Kunihiro, B. Muller, A. Ohnishi, A. Schafer, T. T. Takahashi, and A. Yamamoto, Phys. Rev. **D82**, 114015 (2010), 1008.1156.
- [112] K. Fukushima and F. Gelis, Nucl. Phys. **A874**, 108 (2012), 1106.1396.
- [113] T. Epelbaum and F. Gelis, Phys. Rev. Lett. **111**, 232301 (2013), 1307.2214.
- [114] J. Berges, K. Boguslavski, S. Schlichting, and R. Venugopalan, JHEP **05**, 054 (2014), 1312.5216.
- [115] T. Epelbaum, F. Gelis, and B. Wu, Phys. Rev. **D90**, 065029 (2014), 1402.0115.
- [116] T. Epelbaum, F. Gelis, N. Tanji, and B. Wu, Phys. Rev. **D90**, 125032 (2014), 1409.0701.
- [117] J. Berges, K. Boguslavski, S. Schlichting, and R. Venugopalan, Phys. Rev. **D89**, 074011 (2014), 1303.5650.
- [118] J. Berges, K. Boguslavski, S. Schlichting, and R. Venugopalan, Phys. Rev. **D89**, 114007 (2014), 1311.3005.
- [119] J. Berges, K. Boguslavski, S. Schlichting, and R. Venugopalan, Phys. Rev. Lett. **114**, 061601 (2015), 1408.1670.
- [120] J. M. Luttinger and J. C. Ward, Phys. Rev. **118**, 1417 (1960).
- [121] G. Aarts, D. Ahrensmeier, R. Baier, J. Berges, and J. Serreau, Phys. Rev. **D66**, 045008 (2002), hep-ph/0201308.
- [122] E. A. Calzetta and B. L. Hu (2002), hep-ph/0205271.
- [123] J. Berges, Phys. Rev. **D70**, 105010 (2004), hep-ph/0401172.
- [124] J. Berges, AIP Conf. Proc. **739**, 3 (2005), [3(2004)], hep-ph/0409233.
- [125] G. Baym and L. P. Kadanoff, Phys. Rev. **124**, 287 (1961).
- [126] Y. Hatta and A. Nishiyama, Nucl. Phys. **A873**, 47 (2012), 1108.0818.
- [127] Y. Hatta and A. Nishiyama, Phys. Rev. **D86**, 076002 (2012), 1206.4743.
- [128] T. Epelbaum, F. Gelis, S. Jeon, G. Moore, and B. Wu, JHEP **09**, 117 (2015), 1506.05580.
- [129] P. Bozek, Phys. Rev. **C85**, 014911 (2012), 1112.0915.
- [130] P. Bozek and W. Broniowski, Phys. Lett. **B718**, 1557 (2013), 1211.0845.
- [131] P. Bozek, W. Broniowski, and G. Torrieri, Phys. Rev. Lett. **111**, 172303 (2013).
- [132] K. Werner, B. Guiot, I. Karpenko, and T. Pierog, Phys. Rev. **C89**, 064903 (2014), 1312.1233.
- [133] K. Werner, M. Bleicher, B. Guiot, I. Karpenko, and T. Pierog, Phys. Rev. Lett. **112**, 232301 (2014), 1307.4379.
- [134] P. Bozek and W. Broniowski, Phys. Rev. **C88**, 014903 (2013), 1304.3044.
- [135] I. Kozlov, M. Luzum, G. Denicol, S. Jeon, and C. Gale (2014), 1405.3976.
- [136] S. Schlichting and B. Schenke, Phys. Lett. **B739**, 313 (2014), 1407.8458.
- [137] H. Niemi and G. S. Denicol (2014), 1404.7327.
- [138] A. Kovner and M. Lublinsky, Phys. Rev. **D83**, 034017 (2011), 1012.3398.
- [139] K. Dusling and R. Venugopalan, Phys. Rev. **D87**, 094034 (2013), 1302.7018.
- [140] A. Dumitru, L. McLerran, and V. Skokov, Phys. Lett. **B743**, 134 (2015), 1410.4844.
- [141] T. Lappi, Phys. Lett. **B744**, 315 (2015), 1501.05505.
- [142] T. Lappi, B. Schenke, S. Schlichting, and R. Venugopalan (2015), 1509.03499.
- [143] B. Schenke, S. Schlichting, and R. Venugopalan, Phys. Lett. **B747**, 76 (2015), 1502.01331.
- [144] K. Dusling, W. Li, and B. Schenke (2015), 1509.07939.